Powder Technology 400 (2022) 117234

Contents lists available at ScienceDirect

Powder Technology

journal homepage: www.elsevier.com/locate/powtec

Discharge characteristics of non-gravity-driven powder in horizontal silos

Jie Tang, Haifeng Lu *, Xiaolei Guo, Haifeng Liu

Shanghai Engineering Research Center of Coal Gasification, East China University of Science and Technology, P. O. Box 272, Shanghai 200237, PR China

ARTICLE INFO

Article history:
Received 9 December 2021
Received in revised form 21 February 2022
Accepted 23 February 2022
Available online 26 February 2022

Keywords:
Horizontal silo
Discharge characteristics
Non-gravity-driven
Pressure surcharge limit
Mass flow rate

ABSTRACT

Powder flow inside horizontal silos is essential to ensure the efficient operation of the spacecraft using powder engines under horizontal flight positions. In the present work, the discharge characteristics of non-gravity-driven powder in the horizontal silo were investigated experimentally, with an emphasis on the half cone angle, aeration position, and additional pressure. The experimental results show that the mass flow rate first increases with decreasing half cone angle and then approaches saturation. Aerating at the cylinder was proved to be able to significantly increase the mass flow rate compared with the previous aeration at the cone. Increasing the additional pressure can effectively improve the mass flow rate, but there is a limit value called pressure surcharge limit to maximize the discharge rate. And aerating at the cylinder can further increase the pressure surcharge limit as well as the maximum mass flow rate, which is close to the ideal flow rate based on the liquid-like hypothesis. Finally, an index η is proposed to evaluate the overall flow-promoting effect to determine the optimal aeration position.

1. Introduction

Granular materials are discrete and disordered systems [1] formed by the aggregation of many single particles, and widely exist in nature and industrial production. The complex and interesting phenomena and mechanisms behind them have attracted the inquiry of countless scholars. However, the granular materials in the actual application need to be stored and transported [2], and the silos play a significant role in this process. Therefore, the flow of particulates in the silos has been extensively studied [3,4].

The flow of granular materials driven by gravity in the silos has always been concerned by academia due to its wide industrial application, and the flow pattern [5], stress distribution [6,7], velocity profile [8], and mass flow rate [9] in the silos are the focus of research. However, as the properties of the particles and operating conditions change, local clogging or arch structure may occur in the silos, and the discharge driven by gravity alone cannot be smooth. In this case, extra energy needs to be introduced into the systems, such as mechanical vibration or gas injection. Janda et al. [10] found that for the smaller orifices, the vibration can achieve an intermittent state characterized by alternating cycles of flow and blockage to reach the purpose of discharge. Pascot et al. [11] studied experimentally and numerically the influence of mechanical vibration on the mass flow rate in a quasi-two-dimensional silo and found that vibration would cause two distinct states of flow rate: decrease and increase. Du et al. [12] studied the effect of vibration on the powder discharge in a hemispherical bottom silo and proposed an enhancement factor to evaluate the effect of vertical vibration on improving the emission of particulates. In addition, gas injection is another effective method to promote powder discharge. Lu et al. conducted a series of detailed studies on the aeration characteristics of powder, including the influence of gas types [13] and pressurized aerated silo [14]. Zhu et al. [15] introduced the pulse airflow into the silos firstly to explore the influence of pulse parameters on the discharge of cohesive powder and found that the pulse airflow can effectively increase the mass flow rate and discharge stability compared with the continuous airflow. Ferrari et al. [16] investigated the particle flow inside a two-dimensional aerated hopper and found the transition from the funnel flow to the mass flow is attained at aeration rates smaller than the minimum for fluidization.

It can be found that the above researches are all concentrated in vertical silos. However, with the development of near-earth space and the exploration of outer space, the missions of spacecraft are becoming more diversified and the working environment is more complex and variable. A new type of engine using powder fuel such as aluminum powder as the propellant, namely the powder engine [17,18], has been proposed to accomplish the task. And the supply and fluidized transportation of powder propellant are the key links in the powder engine [19]. Over the past few decades, a variety of powder propellant

* Corresponding author.
E-mail address: luhf@ecust.edu.cn (H. Lu).

https://doi.org/10.1016/j.powtec.2022.117234
0032-5910/

feeding systems have been developed. Despite their structural differences, all require the use of silos to store and transport powder fuel [20]. Therefore, to ensure the high-efficient delivery of powder fuel under the horizontal flight position of spacecraft, it is very important to study and understand the discharge characteristics of powder in the horizontal silos [21]. In addition, the horizontal silo has potential application value where the space height is limited.

Due to the powder discharge direction being perpendicular to the gravity direction, there is a lack of effective driving force to achieve the discharge. In order to discharge the powder smoothly from the horizontal silos and maintain a tight accumulation state, a piston is usually added to the end of the silo and moves with the powder, and the driving force primarily includes the pneumatic-driven piston [22] and motor-driven piston [23] types, which are not needed in the vertical silos. Therefore, the powder flow is also more complicated. However, the researches on the discharge characteristics of powder in the horizontal silos are very few [24,25] and further study is needed.

In this study, experiments were carried out on the effects of the half cone angle, aeration position, and additional pressure on the discharge characteristics of powder in the test horizontal silos with consideration of the mass flow rate and powder utilization rate, which is important to promote the application of horizontal silos in related fields and fill the gap of powder flow in the non-gravity direction.

2. Experimental setup

2.1. Materials

2.1.1. Physical property

Considering that there may be a dust explosion if micro aluminum powder disperses into the air, the neutral glass beads were considered as the experimental materials. As shown in Fig. 1, the cumulative particle size distributions were obtained by a Malvern Laser Particle Size Analyzer (Mastersizer 2000). It can be seen from the figure that glass beads and aluminum have similar particle size distribution with surface area mean size of $d_{32} = 33$ μm and 27 μm respectively. And the basic physical properties of two materials are shown in Table 1, both of which present close physical and flow parameters, including the bulk density ($\rho_{b,\,d}$), tap density (ρ_t), angle of repose (*AOR*), and Carr flow index (*FI*) determined by a PT-X powder tester (Hosokawa Micron Corporation). The particle density (ρ_p) was measured by an automatic true density analyzer (Quantachrome 1200e).

2.1.2. Compressibility, shear, and wall friction test

The FT4 powder rheometer was used to test the compressibility of the both materials to reflect their bulk properties. In the test process,

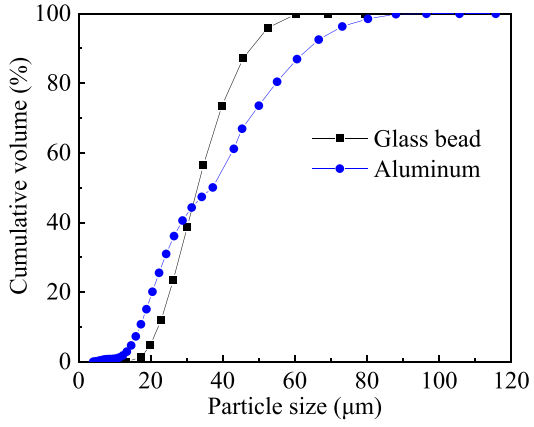

Fig. 1. Cumulative particle size distributions of glass beads and aluminum.

Table 1
Comparison of physical parameters of glass beads and aluminum.

Material	d_{32} (μm)	ρ_p (kg/m^3)	$\rho_{b,\,d}$ (kg/m^3)	ρ_t (kg/m^3)	*AOR* (°)	*FI*
Glass bead	33	2490	1370	1549	32.1	86.5
Aluminum	27	2565	1385	1678	31.7	82.0

the materials in the test vessel were pretreated and split first to ensure them have a uniform volume and stacking state. The condition bulk density (ρ_{CBD}) was obtained. Then, a series of normal stresses from 0.5 kPa to 15 kPa was gradually applied to the materials by a vented piston. Finally, the relationship between the bulk density and the normal stress could be obtained by measuring the volume change of a certain quality of powder materials. The results of the compressibility test are shown in Fig. 2(a). And according to the powder compressibility equation proposed by Tomas [26]:

$$\frac{\rho_b}{\rho_{b,0}} = \left[\frac{\sigma_z + \sigma_{z,0}}{\sigma_{z,0}}\right]^N \tag{1}$$

where $\rho_{b,0}$ is the powder bulk density without normal stress, and $\sigma_{z,0}$ is the pull-off stress when the unconfined yield strength is zero, and N is the compressibility index. Eq. (1) demonstrates the relationship between the bulk density and normal stress, ρ_b (σ_z). N of glass beads and aluminum are 0.019 and 0.024, less than 0.050, indicating that the two materials belong to low compressibility powder.

The shear and wall friction properties of the both materials were also characterized by the FT4 powder rheometer. In the shear test, the critical shear stress value when the powder bed failed was recorded while the shear head applied specified normal stress to the powder bed and began to rotate to induce shear stress after the pretreatment and split procedure. Based on the normal and shear stress collected, the yield locus at a given pre-consolidation condition can be acquired. In the wall friction test, the shear head was replaced by a plexiglass sheet of the same material as the silo and the subsequent procedure was similar to the shear test. The angle of internal friction (φ_i) and the angle of wall friction (φ_w) of glass beads and aluminum were obtained by the above tests and shown in Table 2. (the deviations of the angle of internal friction and angle of wall friction are within ±2° around the average, so the average of the values under various consolidation levels is adopted in this paper). In addition, the unconfined yield strength (f_c) and cohesion (C) of both materials are shown in Fig. 2(b) and (c). These present close rheological parameters of both powders.

However, it could be expected that some differences appear because of the distinct nature of both materials, such as the flammability, chargeability, and hardness. Specifically, aluminum particles are metal, which is combustible and has better chargeability, which is also an important reason for the dust explosion. In addition, it has lower hardness (the Mohs hardness scale of aluminum medium is 2–3, while the Mohs hardness scale of glass medium is 6–7). Nonetheless, the test results of Section 2.1 show that the flowability, compressibility, shear property, and wall friction property of both materials are very close, and it is quite reasonable to assume that the expected behavior of glass beads as the experimental materials would be similar to the aluminum powder.

2.2. Apparatus and procedures

The experimental apparatus used is illustrated in Fig. 3. It is composed of the horizontal silo, the aeration system, and the servo motor control system. The silo is mainly divided into the cylinder section with a length of 400 mm and an inner diameter D of 100 mm, and the cone section with the fixed outlet diameter d of 5 mm and different half cone angle α, which are made of transparent plexiglass. In order to assist the powder discharge, set up multiple rows of aeration vents at the cone and the cylinder respectively. l/L was used to indicate the

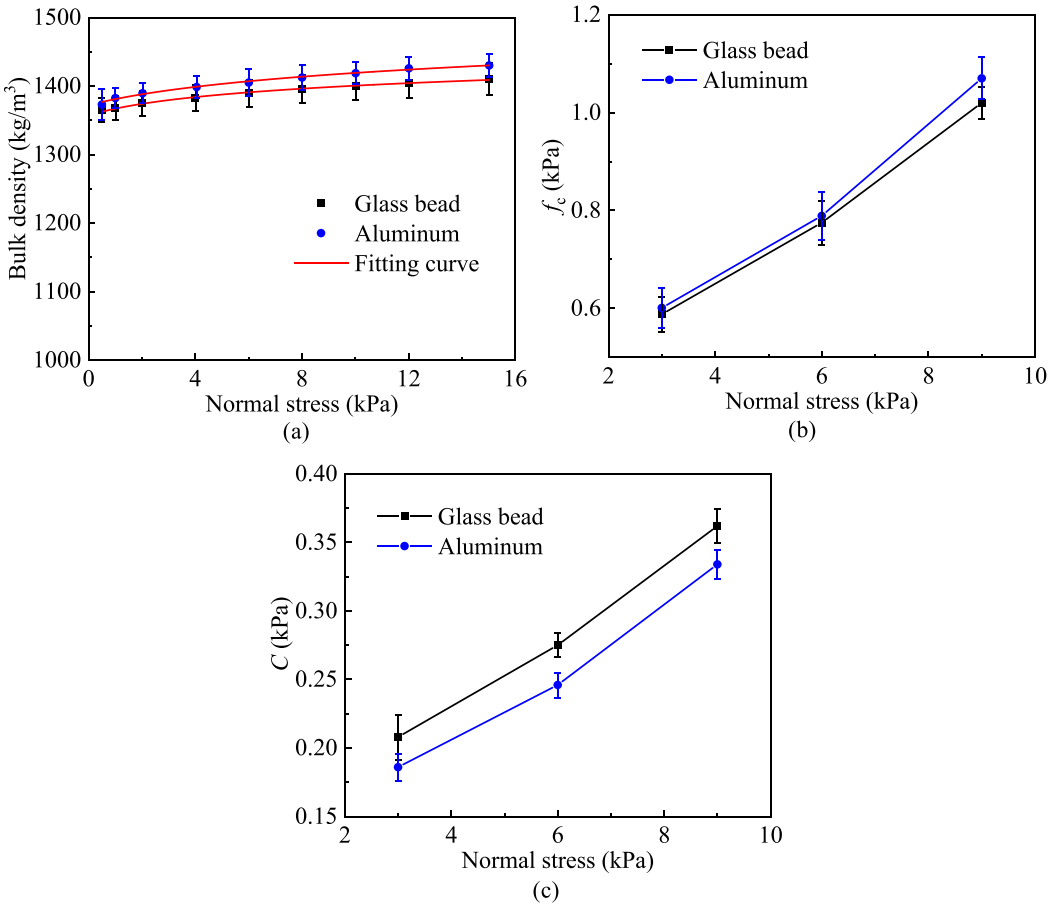

Fig. 2. Relationship between normal stress and: (a) bulk density; (b) unconfined yield strength; (c) cohesion.

Table 2
Angle of internal friction and angle of wall friction of glass beads and aluminum.

Material	σ_{pre} (kPa)	φ'_i (°)	φ'_w (°)	φ_i (°)	φ_w (°)
Glass bead	3	21.8	19.6		
	6	21.6	18.4	21.3	18.6
	9	20.4	17.9		
Aluminum	3	26.4	20.9		
	6	26.2	20.1	26.5	20.0
	9	26.9	19.0		

position of the aeration vents at the cone, where l and L represent the horizontal distance from the aerating position on the cone and junction of cone and cylinder to the outlet respectively. And the specific structural parameters can be found in Table 3. There are three rows at the cylinder, with two adjacent intervals of 50 mm, recorded as B_1, B_2, and B_3 respectively. Each row has four vents and each vent with an internal diameter of 10 mm was inlaid with sintered bronze plates to ensure gas is evenly distributed and avoid particles leakage into the gas pipeline. And the silo was located on an all-metal and rotatable frame

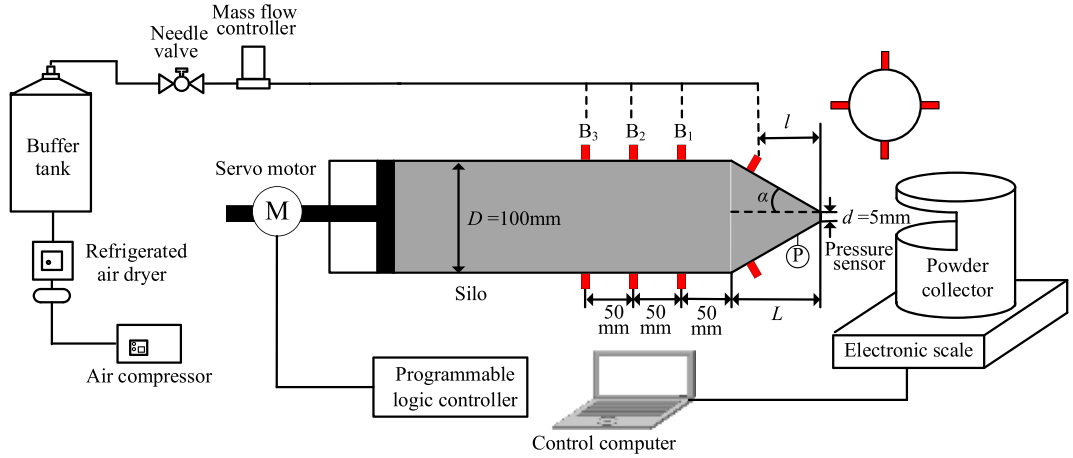

Fig. 3. Schematic diagram of the experimental setup.

Table 3
Structural parameters of the tested silo.

α (°)	L (mm)	l (mm)	l/L
15	177	124	0.7
25	102	71	0.7
30	82	33, 58, 82	0.4, 0.7, 1.0
35	68	48	0.7
45	48	33	0.7
60	27	19	0.7

which was grounded to eliminate the electrostatic effect. Pressurized air was supplied by an air compressor and dried by a freeze dryer. A buffer tank was used to store dry air and as a pressure pulsation equalizer to provide a stable air source. Then a needle valve and a mass flow controller (Qixing Huachuang, CS200) were set up to accurately control the airflow rate (q). A piston is connected with a servo motor (Delta, ECMA-C2060RS) to act on the material surface to provide the additional pressure (σ). The servo motor is controlled by a programmable logic controller and set to torque mode. And the corresponding output torque of the motor shaft is set through the input of external voltage analog quantity to realize the control of the additional pressure acting on the material surface. At the same time, the built-in encoder of the motor sends the feedback signal to the driver, and the driver compares the feedback value with the target value, adjusts the output torque, forms a closed-loop control, and keeps the corresponding additional pressure constant.

When each experiment was carried out, the silo was first rotated to the vertical direction. The powder was loaded into the silo through a sieve to obtain the initial dense column and the length of the powder column in the cylinder is 300 mm. Then a well-airtight piston with the same inner diameter as the cylinder was suspended just above the powder column without additional pressure so that the column was completely fixed, and the initial packing fraction will not change during the rotation of the silo. Then rotate the silo to the horizontal direction and fix it. At the same time as the servo motor started, cut into the fluidized gas. The time series of the weight of the powder discharged from the silo were collected and recorded by an electronic scale (the measuring range is 0-10 kg, the accuracy is 1 g, and the acquisition frequency is 5 Hz) and transmitted to the computer in real-time. The flat diaphragm pressure sensor (PR-35×, the measuring range is 0-150 kPa, the accuracy is 0.05%FS, and the acquisition frequency is 100 Hz) from Keller Company was used to measure the pressure change at $l/L = 0.3$ in the horizontal silo. The minimum number of repetitions required depends on the level of error assumed. The repetition is better to be not less than three. In fact, if there was any problem occurred with the test, the experiment will be repeated again. Therefore, a minimum of three test repetitions was set in our work. Points refer to the average values of 3 sets of reproducible data, error bars are standard deviation.

3. Results and discussion

3.1. Discharge process

It is known that the powder flow driven by the gravity in the open vertical silo can maintain a constant mass flow rate (see Fig. 4(a)), which is not affected by the height of the filling powder. This phenomenon is mainly caused by pressure saturation by the Janssen effect [27]

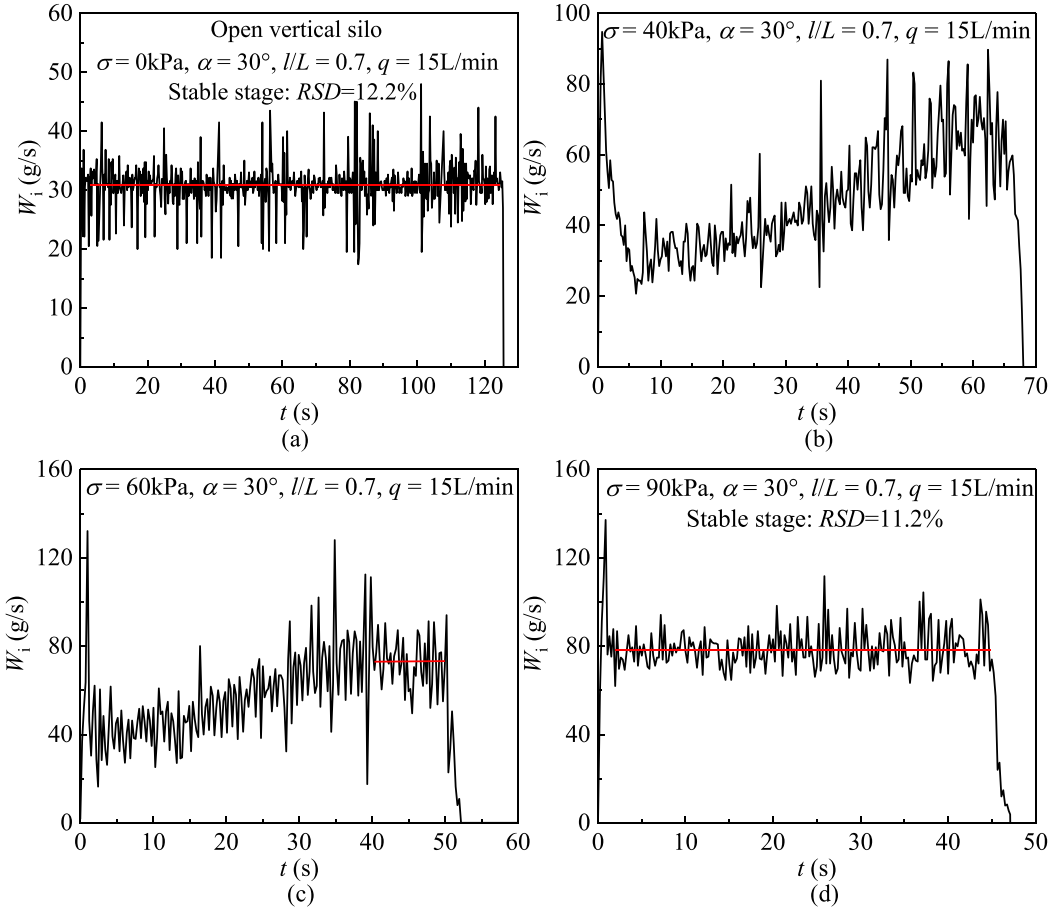

Fig. 4. Instantaneous mass flow rate curve: (a) open vertical silo; (b) (c) (d) horizontal silo with a well-airtight piston under different additional pressures.

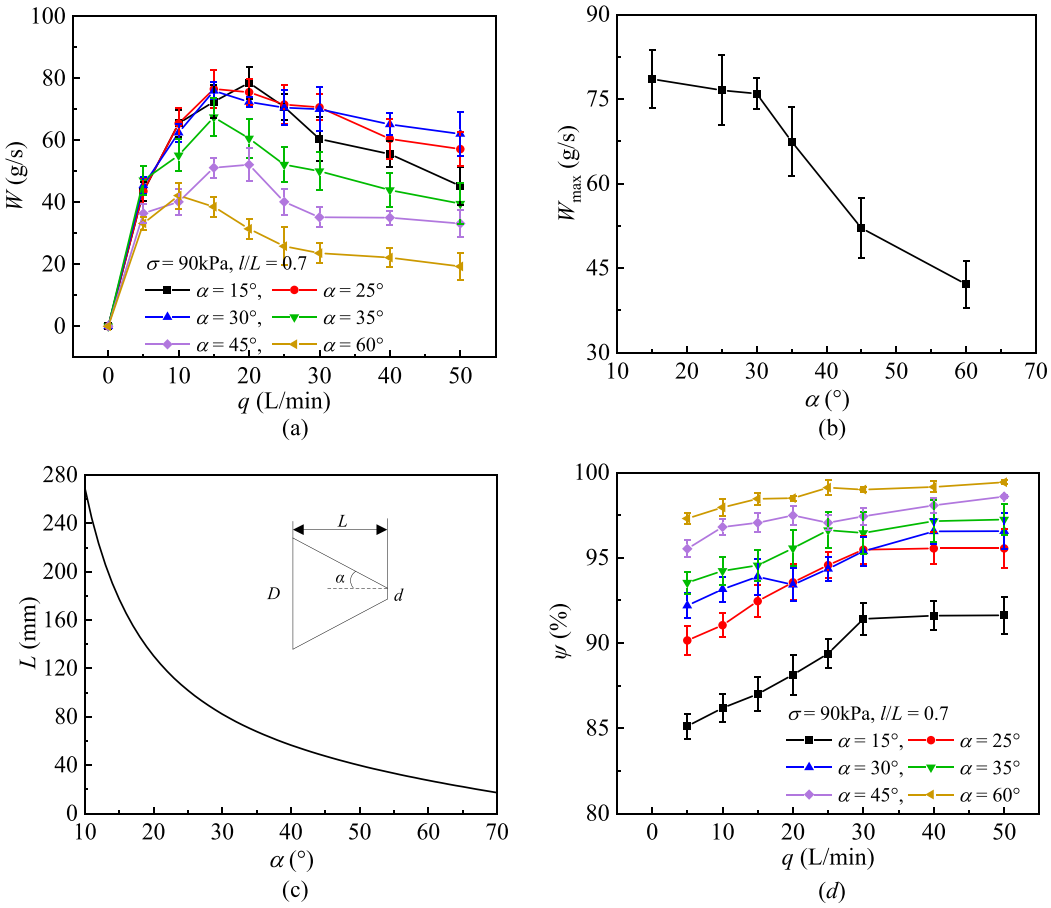

Fig. 5. When different half cone angles are applied: (a) mass flow rate; (b) maximum mass flow; (c) length of the cone; (d) powder utilization rate.

and arch structure [28] near the outlet. Fig. 4(b–d) shows the instantaneous mass flow rate curve of the powder during the entire discharge process under different additional pressures in the horizontal silo. When the additional pressure is relatively small ($\sigma = 40$ kPa), the instantaneous mass flow rate gradually increases. When the σ is increased to 60 kPa, the instantaneous mass flow rate increases first and then remains constant with the reduction of the length of the powder column. When σ is further increased to 90 kPa, the instantaneous mass flow rate remains constant. This may be the changes of additional pressure enhance the degree of frictional mobilization in the silo [29,30], increasing the friction between particles and between particles and the wall, saturating the pressure near the outlet.

It is worth noting that the powder in the horizontal silo is mainly pushed by the piston. For aerating at the cone, when the piston travels to the junction of the cone and cylinder or near the junction, it will stop moving forward. At this time, due to the gravity, some powder will be deposited at the bottom of the cone and not be discharged smoothly only by airflow, which is not conducive to the maximum utilization of powder and different from the vertical silo.

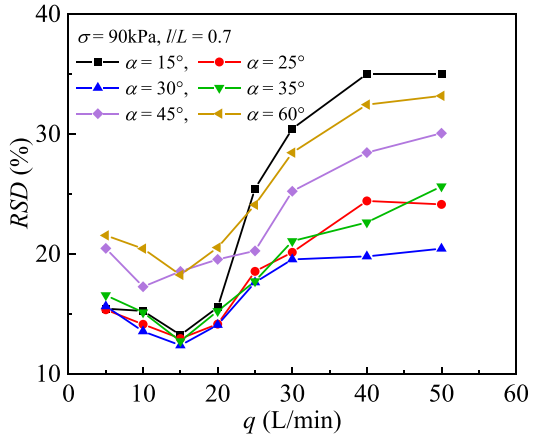

Fig. 6. *RSD* of mass flow rate under different half cone angles.

3.2. Effect of half cone angle

To facilitate the comparison and analysis below, we uniformly take the ratio of the powder outflow mass (Δm) and time Δt in the whole discharging process as the mass flow rate (W), and the ratio of the mass of discharged powder to the total mass of powder loaded as the powder utilization rate (ψ).

The half cone angle is always regarded as an important parameter in the design of silo structure, so its influence on discharge characteristics of powder in the horizontal silo was investigated in this section. And the aeration positions of different half cone angles all satisfy $l/L = 0.7$ to maintain the comparability of the experimental data as much as possible.

Fig. 5(a) demonstrates the experimental results of the mass flow rate under different half cone angles. In fact, the particles will squeeze each other under the additional pressure of the motor due to the reduction of the cross-sectional area of the cone, resulting in a compression arch to bear the additional pressure and hinder the discharge of powder.

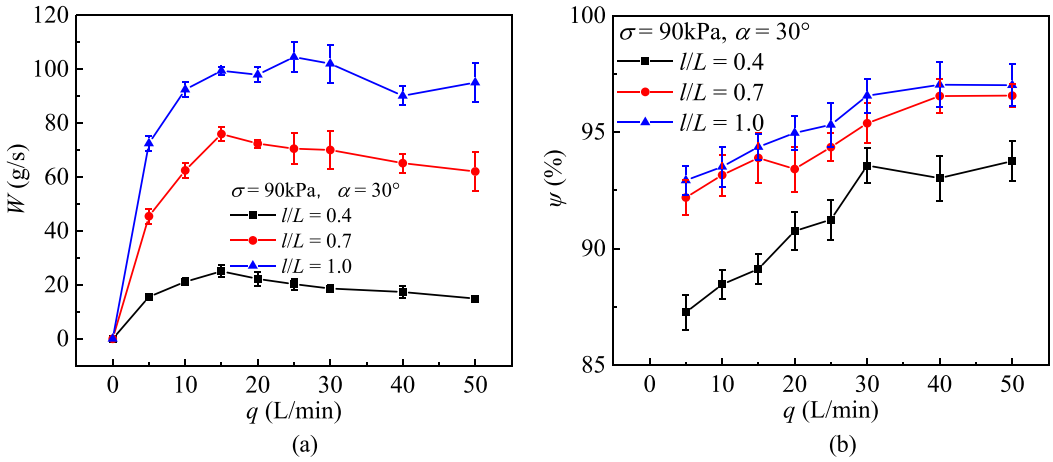

Fig. 7. When aerating at the cone: (a) mass flow rate; (b) powder utilization rate.

Therefore, the powder can only rely on internal slippage to be extruded in a very small amount or not without the assistance of the airflow, and the mass flow rates at this time are all considered to be zero.

What's more, at all half cone angles, the mass flow rate increases first and then decreases with the increase of airflow rate, which means that there is a maximum mass flow rate caused by the change of airflow rate. On the one hand, the introduction of airflow will enhance the flowability of the powder. On the other hand, further increasing the airflow rate will reduce the powder concentration at the outlet. The results in Fig. 5(b) also present that this maximum mass flow rate increases gradually with decreasing the half cone angle and then approaches saturation at 30°. Gas drag force is an important factor in making particles move. And the volume of the cone becomes larger due to the decrease of the angle, so the residence time of the airflow in the silo and the space where the powder is fluidized increase, and the momentum and heat exchange between the gas and the particles are more sufficient to improve the mass flow rate. However, further reduction of the half cone angle will significantly increase the length of the cone (see Fig. 5(c)) and increase the collision probability between particles and particles and between particles and the cone wall, so that the smaller half cone angle improves the mass flow rate not obvious. Fig. 5(d) shows that the reduction of the half cone angle increases the bottom space of the hopper, which results in more powder residue and reduces the powder utilization rate.

The relative standard deviation (*RSD*) of the mass flow rate is compared and analyzed to characterize the degree of deviation from the average value, and the results are shown in Fig. 6. When the half cone angle changes from 60° to 30°, the decrease of the angle can increase the stability of the discharge. Different from the vertical silo, powder in the cone is unevenly distributed in the radial direction due to gravity, which makes the gas main in the upper space, causing stronger gas turbulence. As the half cone angle decreases from 30° to 15°, the momentum exchange between the airflow and the particles is more sufficient, but the space for the action of gas turbulence is also further increased and the strength of gas turbulent becomes more significant, and discharge stability is worse and varies greatly with air flow rate, which will seriously affect the security of the operation of the system. And this is an important reason that the mass flow rate decreases with the reduction of the half cone angle when it is in the range of 30° ~ 15° and the airflow rate is larger.

The above results show that it is not advisable to reduce the half cone angle arbitrarily. Therefore, the half cone angle of 30° is recommended in the actual application and is mostly taken as the object of discussion in this paper based on the consideration of mass flow rate, powder utilization rate, and discharge stability.

3.3. Effect of aeration position

3.3.1. Aeration at the cone

The mass flow rate is not only related to the half cone angle but also has a close relationship with the aeration position. As can be seen from Fig. 7, When the aeration position at the cone is far away from the outlet,

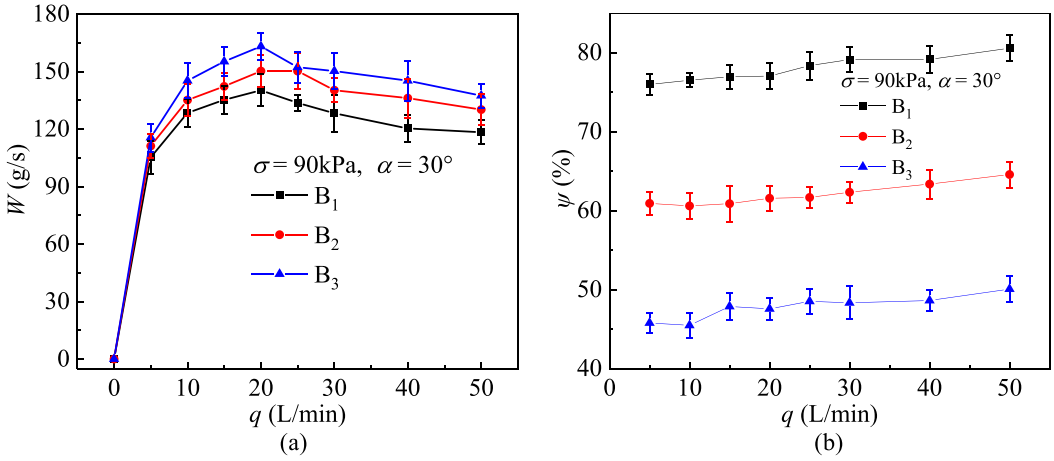

Fig. 8. When aerating at the cylinder: (a) mass flow rate; (b) powder utilization rate.

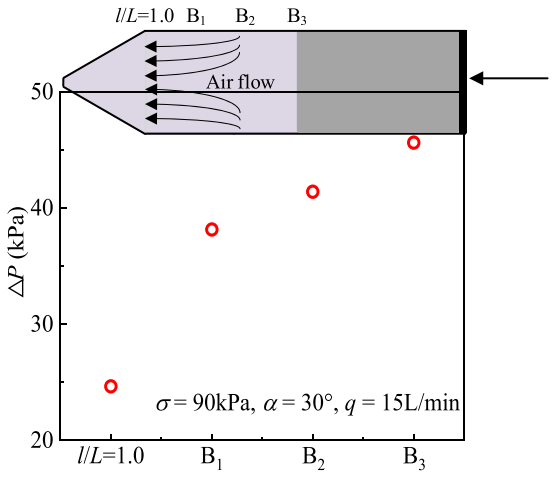

Fig. 9. Average pressure difference at $l/L = 0.3$ under different aeration positions.

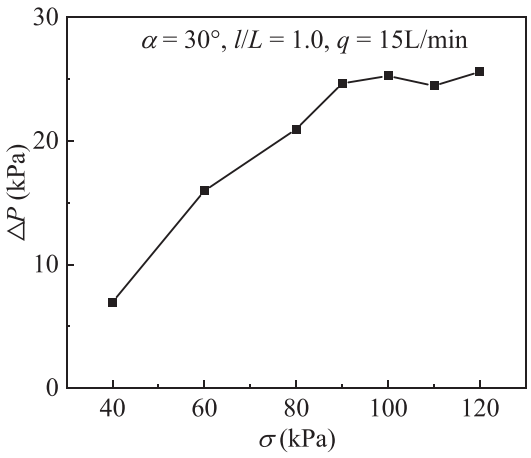

Fig. 11. Average pressure difference at $l/L = 0.3$ under different additional pressures.

not only can a higher mass flow rate be achieved, but also the airflow will sweep out more powder in front of it to improve the powder utilization rate. And the position satisfying $l/L = 1.0$ can also be considered the best position for aerating at the cone.

3.3.2. Aeration at the cylinder

In the past, the aeration position was mainly concentrated at the cone [15], while the aeration position at the cylinder has never been discussed. Fig. 8 shows that the mass flow rate is higher when the aeration position at the cylinder is further away from the outlet. However, the piston stops moving when it reaches the aeration position, the airflow escapes, and the powder is no longer discharged. So, the more powder residue quality at the end of the discharge. In addition, it is found that aerating at the cylinder can achieve a more pronounced flow-promoting effect but a lower powder utilization rate than that of aerating at the cone.

For the horizontal silo, the effective driving force of the discharge flow without the consideration of the gravity can be the pressure difference ΔP. Fig. 9 shows the average pressure difference at $l/L = 0.3$ under each aeration position. Due to the necessary well-airtight piston and additional pressure in the horizontal silos, the airflow is more inclined to flow toward the outlet. Therefore, aerating at the cylinder can enlarge the action space of airflow, enhance the flowability of more powder and reduce the friction resistance between the powder and the wall of the silo to make additional pressure transmit efficiently. The above reasons also make the pressure difference near the outlet under aerating at the cylinder larger than that under aerating at the cone, so the energy of particles near the outlet is larger to obtain a higher mass flow rate.

3.4. Effect of additional pressure

Further, the influence of additional pressure which is the main driving force on the discharge characteristics of powder in the horizontal silo was investigated, as shown in Fig. 10. The results demonstrate that increasing the additional pressure within a certain range can effectively increase the mass flow rate, such as 40–90 kPa. But when the additional pressure further increases, the mass flow rate basically does not change, that is, there is a pressure surcharge limit of $\sigma_s = 90$ kPa maximizing the mass flow rate.

Similar to measurement of the pressure under different aeration positions, here the experiments under different additional pressures were completed, as shown in Fig. 11. Due to the change of the front and back cross-sectional area of the junction of cone and cylinder, the powder with low compressibility under the influence of additional pressure is likely to form a compression arch at the junction. When the additional pressure is small, the compression arch formed at the cone has low strength and a weak hindrance to the flow of powder. With the continuous improvement of additional pressure, the pressure increases gradually, indicating that the driving force transferred to the vicinity of the

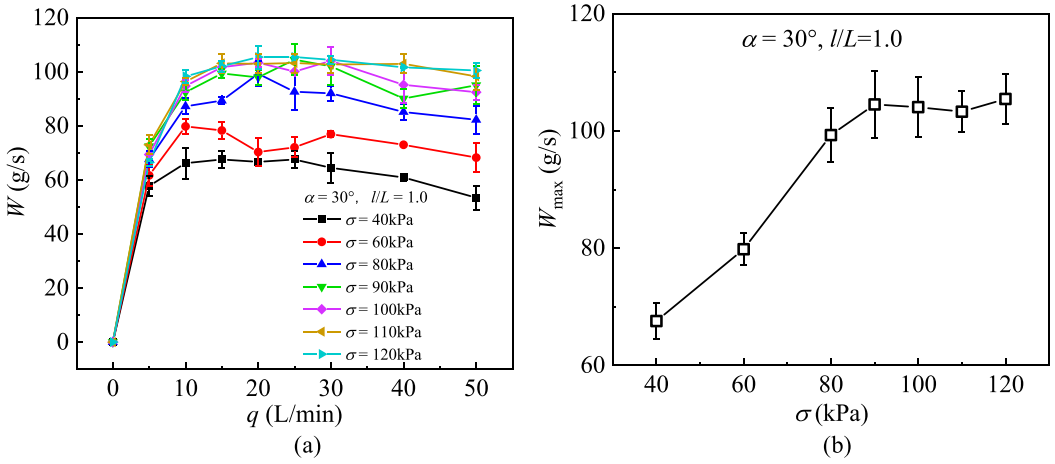

Fig. 10. Mass flow rate under different additional pressures when aerating at $l/L = 1.0$.

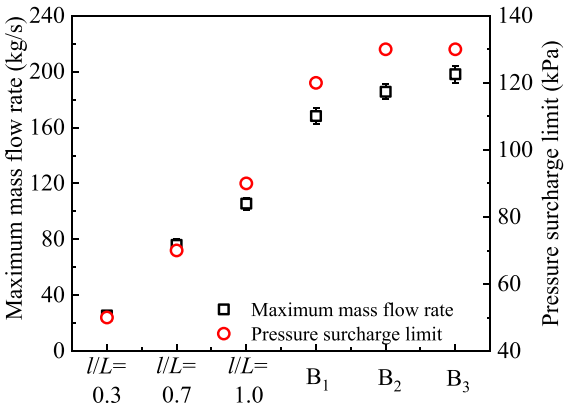

Fig. 12. Pressure surcharge limit and maximum mass flow rate under different aeration positions with $\alpha = 30°$.

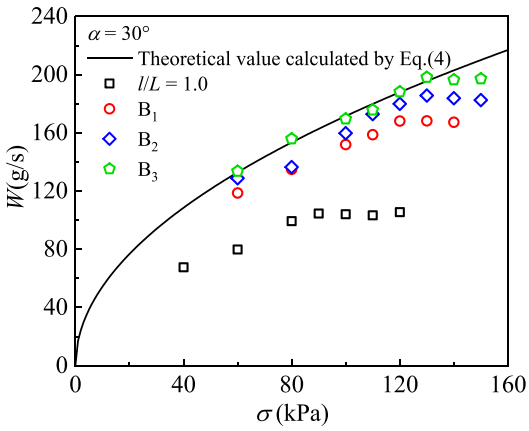

Fig. 14. Comparison of the enhancement effect.

outlet is also greater, so the energy of the powder particles at the outlet is also increasing, and the mass flow rate has been significantly improved. However, when the additional pressure increases to a certain value, the f_c of the powder will increase to enhance the strength of the arch. And most of the additional pressure will be borne by the arch to cause the pressure difference to remain almost constant and the energy of particles at the vicinity of the outlet will no longer increase with the increase of the additional pressure, resulting in no significant change in the mass flow rate.

According to the above results, the pressure surcharge limit hinders the further improvement of the mass flow rate. And for aeration at the cone, the maximum mass flow rate is about 105 g/s. However, the results in Fig. 12 present that the maximum mass flow rate can be increased to about 200 g/s by aerating at B_3 on the cylinder by increasing the pressure surcharge limit.

3.5. Evaluation of flow-promoting effect

Since the gas only flows out of the silo from the outlet and the compression arch forms near the junction of the cylinder and cone under the action of the additional pressure, only the powder in the cone can be well fluidized. Therefore, as shown as in Fig. 13, the silo is divided into 3 sections in the case, assuming that Sections 1–2 and 2–3 are the dense phase moving area and the free flow area respectively.

The preliminary work [31] shows that the axial pressure changes of the powder at Sections 1–2 can be obtained from $P_2 = P_1 \exp(-4\mu_w K \frac{L_p}{D})$, where P_1 and P_2 are the axial pressures of Sections 1 and 2, respectively, μ_w is wall friction coefficient ($\mu_w = \tan\varphi_w$), K is the pressure transmission coefficient ($K = (1\text{-}\sin\varphi i)/(1 + \sin\varphi i)$), and L_p is the powder length of Sections 1–2. Then, for Sections 2–3, the law of conservation of energy can be obtained:

$$P_2 + \frac{\rho_{b,0} u_2^2}{2} = P_3 + \frac{\rho_{b,0} u_3^2}{2} + \zeta_c \frac{\rho_{b,0} u_3^2}{2} \tag{2}$$

The axial pressures of Sections 1 and 3 are $P_1 = \sigma$ and $P_3 = 0$ kPa, respectively. u_2 and u_3 are the powder velocities of Sections 2 and 3,

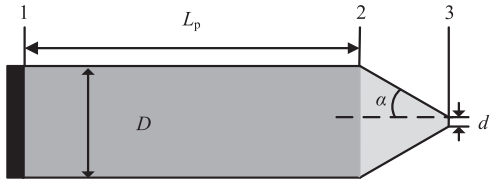

Fig. 13. Diagram of the horizontal silo.

respectively, where $u_2 = u_3 \frac{A_3}{A_2} = u_3 \frac{d^2}{D^2}$ and $\frac{\rho_{b,0} u_2^2}{2}$ can be ignored due to $d^2 \ll D^2$. ζ_c is the local resistance coefficient (Sections 2–3 can be regarded as fluidization and thus fluid-like, so $\zeta_c = 0.8 \sin(\alpha)(1-\frac{d^2}{D^2})$). Since L_P is continuously reduced during the discharge process and $L_p/D \le 3$, in order to simplify the calculation, we take $\bar{L}_p = \frac{L_p}{2}$ into Eq. (2):

$$u_3 \approx \frac{1}{\sqrt{1+\zeta_c}} \sqrt{\frac{2\sigma \exp\left(-4\mu_w K \frac{L_p}{2D}\right)}{\rho_{b,0}}} \tag{3}$$

So the ideal mass flow rate is calculated by the following equation:

$$W = \frac{\pi \rho_{b,0} u_3 d^2}{4} \tag{4}$$

The ideal mass flow rate obtained does not satisfy the analysis of particle flow in a physical sense, but it is used as a benchmark and compare it with experiments to illustrate the flow enhancement effect. The comparison of experimental and theoretical values is presented in Fig. 14, and both have similar change trends. When aerating at the cylinder, the air flow can act on the powder in Sections 2–3 to improve the fluidity of more powder to make the transition from Sections 1–2 to 2–3 closer to the assumption. Therefore, before reaching the saturation pressure, the experimental results of aerating at the cylinder are very close to the theoretical value and the flow-promoting effect is excellent.

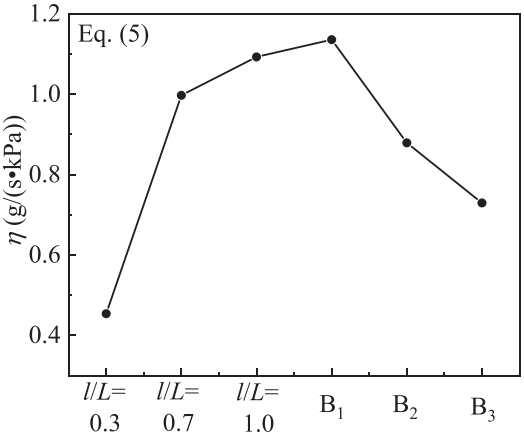

Fig. 15. Overall flow-promoting effect of each aeration position for $\alpha = 30°$.

Finally, an index η is proposed to evaluate the overall flow-promoting effect of each aerating position:

$$\eta = \frac{W_{max}}{\sigma_s}\psi \quad (5)$$

where W_{max} is the maximum flow rate under pressure surcharge limit σ_s, ψ is the powder utilization rate under corresponding working conditions. As shown in Fig. 15, η increases firstly and then decreases with the increase of distance between the aeration position and the outlet, where B_1 is the best position in the experiments.

4. Conclusion

In summary, the influences of airflow rate, half cone angle, aeration position, and additional pressure on discharge characteristics of non-gravity-driven powder in the horizontal silos were investigated. The main findings of this study were summarized in the following conclusions:

(1) The mass flow rate firstly increases and then decreases with the increase of airflow rate. In addition, the maximum mass flow rate caused by the change of airflow rate first increases with the decrease of half cone angle and then approaches saturation at half cone angle of 30°, which has a high mass flow rate and good discharge stability.
(2) Aerating at the cylinder by optimizing the pressure transmission of the powder bed to obtain a substantial increase in the mass flow rate compared with that of previous aerating at the cone.
(3) There is a limit value called pressure surcharge limit to maximize the flow rate for each aeration position, indicating that increasing the additional pressure is only effective in a certain range. What's more, aerating at the cylinder can enhance the maximum mass flow rate compared with aerating at the cone by increasing the pressure surcharge limit.
(4) The ideal mass flow rate is estimated based on the liquid-like hypothesis, which shows that aerating at the cylinder has an excellent flow-promoting effect. An index η based on the consideration of mass flow rate, powder utilization rate, and pressure surcharge limit is proposed to determine that B_1 is the optimal aeration position.

CRediT authorship contribution statement

Jie Tang: Conceptualization, Methodology, Writing – original draft, Investigation, Writing – review & editing. **Haifeng Lu:** Writing – review & editing, Formal analysis. **Xiaolei Guo:** Visualization, Investigation, Supervision. **Haifeng Liu:** Validation, Project administration, Funding acquisition.

Declaration of Competing Interest

The authors declare that they have no known competing financial interests or personal relationships that could have appeared to influence the work reported in this paper.

Acknowledgments

The authors acknowledge financial supports from the National Natural Science Foundation of China (51876066) and Shanghai Engineering Research Center of Coal Gasification (18DZ2283900).

References

[1] G.D.R. Midi, On dense granular flows, Europ. Phys. J. E. 14 (2004) 341–365.
[2] A. Cowell, D. McGlinchey, R. Ansell, Determination of pneumatic transport capabilities of dry pulverised coal suitable for entrained flow processes, Fuel. 84 (2005) 2256–2266.
[3] Z. Guo, X. Chen, H. Liu, H. Chen, Gravity discharge characteristics of biomass-coal blends in a hopper, Fuel. 125 (2014) 137–143.
[4] C. Perge, M. Aguirre, P. Gago, L. Pugnaloni, D. Tourneau, J. Géminard, Evolution of pressure profiles during the discharge of a silo, Phys. Rev. E 85 (2012) 021303.
[5] S. Volpato, R. Artoni, A.C. Santomaso, Numerical study on the behavior of funnel flow silos with and without inserts through a continuum hydrodynamic approach, Chem. Eng. Res. Des. 92 (2014) 256–263.
[6] A. Jenike, Steady gravity flow of frictional-cohesive solids in converging channels, J. Appl. Mech. 31 (1964) 5–11.
[7] A. Jenike, A theory of flow of particulate solids in converging and diverging channels based on a conical yield function, Powder Technol. 50 (1987) 229–236.
[8] N. Wang, J. Xu, X. Guo, H. Lu, H. Zhao, H. Liu, Velocity profiles of avalanches during hopper discharge, Fuel. 218 (2018) 350–356.
[9] D. Barletta, G. Donsi, G. Ferrari, M. Poletto, P. Russo, Solid flow rate prediction in silo discharge of aerated cohesive powders, AICHE J. 53 (2007) 2240–2253.
[10] A. Janda, D. Maza, A. Garcimartín, E. Kolb, E. Clément, Unjamming a granular hopper by vibration, Europhys. Lett. 87 (2009) 24002.
[11] A. Pascot, N. Gaudel, S. Antonyuk, J. Bianchin, Influence of mechanical vibrations on quasi-2D silo discharge of spherical particles, Chem. Eng. Sci. 224 (2020) 115749.
[12] J. Du, C. Liu, C. Wang, P. Wu, Discharge of granular materials in a hemispherical bottom silo under vertical vibration, Powder Technol. 372 (2020) 128–135.
[13] H. Lu, X. Guo, X. Gong, X. Cong, W. Dong, W. Huang, Effect of gas type on the fluidization and discharge characteristics of the pulverized coal, Powder Technol. 217 (2012) 347–355.
[14] H. Lu, X. Guo, X. Gong, K. Liu, X. Sun, K. Xie, X. Gong, J. Lu, The discharge of pulverized coal from a pressurized aerated hopper, Ind. Eng. Chem. Res. 51 (2012) 13839–13845.
[15] L. Zhu, H. Lu, M. Poletto, H. Liu, Z. Deng, Hopper discharge of cohesive powders using pulsated airflow, AICHE J. 66 (2020) 16240.
[16] G. Ferrari, M. Poletto, The particle velocity field inside a two-dimensional aerated hopper, Powder Technol. 123 (2002) 242–253.
[17] W. Parsons, E. Forman, Experiments with powder motors for rocket propulsion by successive impulses, Astronautics. 9 (1939) 4–11.
[18] S. Goroshin, Powdered metals as fuel for hypersonic ramjets, 37th AIAA/ASME/SAE/ASEE Joint Propulsion Conference & Exhibit, 2001.
[19] C. Li, C. Hu, X. Xin, Y. Li, Experimental study on the operation characteristics of aluminum powder fueled ramjet, Acta Astronaut. 129 (2016) 74–81.
[20] Y. Li, C. Hu, Z. Deng, C. Li, Experimental study on multiple-pulse performance characteristics of ammonium perchlorate/aluminum powder rocket motor, Acta Astronaut. 133 (2016) 455–466.
[21] M. Meyer, Powdered aluminum and oxygen rocket propellants: subscale combustion experiments, NASA Technical Memorandum, 1993.
[22] J. Foote, R. Litchford, Powdered magnesium: carbon dioxide combustion for mars propulsion, 41st AIAA/ASME/SAE/ASEE Joint Propulsion Conference & Exhibit, 2005.
[23] T. Miller, J. Herr, Green rocket propulsion by reaction of Al and Mg powders and water, 40th AIAA/ASME/SAE/ASEE Joint Propulsion Conference and Exhibit, 2014.
[24] H. Sun, C. Hu, X. Zhu, J. Yang, Experimental investigation on incipient mass flow rate of micro aluminum powder at high pressure, Exp. Thermal Fluid Sci. 83 (2017) 231–238.
[25] H. Sun, C. Hu, T. Zhang, Z. Deng, Experimental investigation on mass flow rate measurements and feeding characteristics of powder at high pressure, Appl. Therm. Eng. 39 (2016) 2853–2862.
[26] J. Tomas, Product design of cohesive powders – mechanical properties, compression and flow behavior, Chem. Eng. Technol. 27 (2010) 605–618.
[27] S. Mahajan, M. Tennenbaum, S. Pathak, D. Baxter, X. Fan, P. Padilla, C. Anderson, A. Fernandez-Nieves, M. Ciamarra, Reverse janssen effect in narrow granular columns, Phys. Rev. Lett. 124 (2020) 128002.
[28] L. Staron, P.Y. Lagrée, S. Popinet, The granular silo as a continuum plastic flow: the hour-glass vs the clepsydra, Phys. Fluids 24 (2012) 103301.
[29] L. Vanel, Ph. Claudin, J.-Ph. Bouchaud, M. Cates, E. Clément, J. Wittmer, Stresses in silos: comparison between theoretical models and new experiments, Phys. Rev. Lett. 84 (2000) 1439–1442.
[30] G. Ovarlez, C. Fond, E. Cle'ment, Overshoot effect in the Janssen granular column: a crucial test for granular mechanics, Phys. Rev. E 67 (2003) 060302.
[31] J. Tang, H. Lu, X. Guo, H. Liu, Static wall pressure distribution characteristics in horizontal silos, Powder Technol. 393 (2021) 342–348.